chemistry proceedings

MDPI

Proceeding Paper

Stokesia laevis Ethanolic Extract Activity on the Normal and Malignant Murine Cell Line Viability L969 and B16 †

Georgeta Neagu, Amalia Stefaniu, Bujor Albu, Iulian Terchescu, Lucia Pintilie and Lucia Camelia Pirvu *

National Institute for Chemical-Pharmaceutical Research and Development, 112 Vitan Av., 031299 Bucharest, Romania; getabios@yahoo.com (G.N.); astefaniu@gmail.com (A.S.); abujor@gmail.com (B.A.); iulianterchescu@yahoo.com (I.T.); lucia.pintilie@gmail.com (L.P.)

* Correspondence: lucia.pirvu@yahoo.com (L.C.P.)

† Presented at the 24th International Electronic Conference on Synthetic Organic Chemistry, 15 November–15 December 2020; Available online: https://ecsoc-24.sciforum.net/.

Abstract: *Stokesia laevis* (common name Stokes aster) ethanolic extract (Slae26) containing 5 mg GAE/mL extract was investigated to establish cytotoxicity and anti-proliferative effects. The assays were performed on normal murine fibroblast cell line L929 and malignant murine melanoma cell line B16, respectively; for the first time in literature data, potential cytotoxic and anti-proliferative effects of the ethanolic extract from *S. laevis* on both, normal murine fibroblast cell line L929, and murine melanoma cell line B16 have been proved. The study is supplemented by molecular docking simulations of the major components of Slae26 against human tyrosinase receptor, to evaluate possible melanogenesis inhibition.

Keywords: stokes aster ethanolic extract; cytotoxicity; anti-proliferative activity; melanogenesis

Citation: Neagu, G.; Stefaniu, A.; Albu, B.; Terchescu, I.; Pintilie, L.; Pirvu, L. *Stokesia laevis* Ethanolic Extract Activity on the Normal and Malignant Murine Cell Line Viability L969 and B16. *Chem. Proc.* **2021**, *3*, 42. https://doi.org/10.3390/ecsoc-24-08318

Academic Editors: Julio A. Seijas and M. Pilar Vázquez-Tato

Published: 14 November 2020

1. Introduction

According to the specialized data, the cutaneous malignant melanoma is the most aggressive type of skin cancer [1]. Data also indicate that the skin melanoma is the most commonly occurring cancer worldwide; the most affected are Australian and New Zealand peoples, followed by Caucasian peoples [2]. Due to high aggressiveness and chemical therapy resistance [3], there are many attempts to find new therapy combinations and antitumor agents or synergistic compounds able to fight against skin melanoma cancer resistance. Among these, several plant species and specific plant compounds indicated promising results, inhibitory activity by in vitro testing of human and murine melanoma cell lines and murine melanoma models, respectively [4].

Aiming to extend the authors' previously published work [5], the present paper aims to study the cytotoxic and anti-proliferative potential of the standardized ethanolic extract (Slae26) from *Stokesia laevis* (J. Hill, fam. Asteraceae), 5 mg GAE/mL extract, on normal murine fibroblast cell line L929 and malignant murine melanoma cell line B16, respectively; the predominant compounds in Slae26 (HPTLC analysis) are caffeic acid and luteolin derivates [5].

2. Materials and Methods

Briefly, the test vegetal extract was obtained from dried and powdered aerial part of *S. laevis* extracted with 70% (*v*/*v*) ethanol at the boiling temperature. The resulted ethanolic extract was analyzed concerning quantitative and qualitative aspects [5], then prepared as standardized 5 mg total phenols content expressed as gallic acid derivates

[GAE] per 1 mL 40% ethanol solution, *v*/*v*, namely Slae26; the Slae26 dilution series (0.5, 1, 5, 10, 25, 50 and 100 μg GAE/mL, test vegetal samples) and corresponding 40% ethanol solvent dilution series (0.04, 0.08, 0.8, 2, 4 and 8% ethanol, *v*/*v*, control samples) were used for further in vitro cell studies.

The in vitro cytotoxicity and anti-proliferative assays were done according to the Technical Bulletin of *Promega Corporation CellTiter 96 AQueous One solution Cell Proliferation Assay* as described in previous study [5]. Briefly, after 20 h (cytotoxicity test) and, respectively, 20 and 44 h (antiproliferative test) of cell exposure, the absorbance of the test samples (Slae26 dilution series) face to control sample (40% ethanol dilution series) were measured at 490 nm (using Chameleon V Plate Reader, LKB Instruments, Mount Waverley, Australia). The recorded values were used for the estimation of the cell viability (see Equation (1)). Results are calculated as mean ± SD, $n = 3$.

$$\%\ \text{cell viability} = \frac{A490\ of\ treated\ cells}{A490\ of\ control\ cells} 100 \quad (1)$$

The molecular docking study was realized using CLC Drug, Discovery Work Bench. Protein fragment, human tyrosinase related protein 1 [6] in complex with kojic acid (PDB ID 5M8M) [7] was imported from Protein Data Bank. Ligands' structures, components of Slae26 (Caffeic acid, Chlorogenic acid, Luteolin, Luteolin-5-*O*-glucoside, Luteolin-7-*O*-glucoside, Luteolin-6-C-glucoside, Luteolin-8-C-glucoside, Luteolin-7,3′-di-*O*-glucoside and Luteolin 3,4′-di-*O*-glucoside) were imported from PubChem (https://pubchem.ncbi.nlm.nih.gov, accessed on 5 November 2020), and docked into 107.01 $Å^3$ binding pocket.

3. Results

3.1. Cytotoxicity and Anti-Proliferative Assays

Figure 1 shows the results on the *Slae26* dilution series tested on (a) murine fibroblast cell line L929 and (b) murine melanoma cell line B16, compared to the control negative cell series (40% ethanol solvent series). Therefore, the cytotoxicity test on the normal murine fibroblast cell line L929 indicated that Slae26 test sample concentrations less than 25 μg/mL induced moderate stimulating effects on the L929 cell line viability (up to 20% increase), after that there were noticed augmented inhibitory activity (up to 84% cell viability decrease at 100 μg/mL); the anti-proliferative test indicated that, less than 10 μg/mL extract at 24 h/h, and less than 5 μg/mL at 48 h, Slae26 induced stimulating effects (up to 25%, and up to 7% cell viability increase, respectively), after which the same decrease in cell viability was observed (inhibition of cell viability up to 65% and 81%, at 24 h and 48 h, respectively).

In the case of malignant murine melanoma cell line B16, the cytotoxicity test shown the same stimulating effects on the B16 cell line viability (up to 8% stimulation of cell viability at the test sample concentrations less than 10 μg/mL), followed by a severe decrease in cell viability at higher concentrations (up to 90% cell viability decrease at 100 μg/mL); similarly, the anti-proliferative test indicated less than 10 μg/mL extract at 24 h, and less than 5 μg/mL at 48 h, Slae26 extract induced stimulating effects on B16 cell line viability (up to 20% and up to 18%, at 24 h and 48 h, respectively), followed by a sharp decrease in cell viability at 24 and 48 h (up to 79% and up to 93% inhibition of cell viability at 24 h and 48 h at 100 μg/mL, respectively).

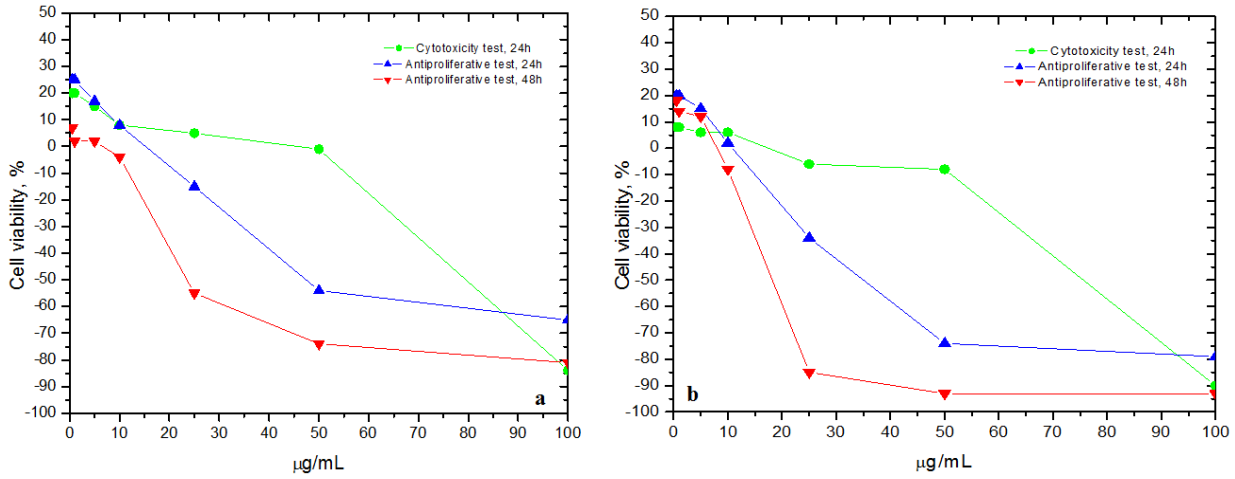

Figure 1. Cytotoxic and antiproliferative effects (cell viability, %) of Slae26 dilution series tested on (**a**) murine fibroblast cell line L929 and (**b**) murine melanoma cell line B16, compared to control negative cell lines (40% ethanol solvent series); $n = 3$, ±SD (%).

3.2. Molecular Docking Results

All investigated structures reveal greater docking score than the co-crystallized ligand (kojic acid). The chart of obtained values for docking score is presented in Figure 2. The best result is given for L-7-*O*-glucoside (66.76). For all compounds, the interactions as hydrogen bond type and length formed with the amino acids residues form the active binding site of the tyrosinase, are listed in Table 1, along with results obtained for the natural ligand (KOJ A514 = Kojic acid). Two of hydrogen bonds interactions formed with the same amino acid residues, as kojic acid forms, SER394 and HIS215, respectively, occur in the complexes of investigated ligands with human tyrosinase related protein 1 fragment, excepting di-glucosides (L-3′,4′-di-*O*-glucoside and L-3′,4′-di-*O*-glucoside). Only HIS215 is present in their interacting amino acids group, but don't establish interactions with the di-glucosides.

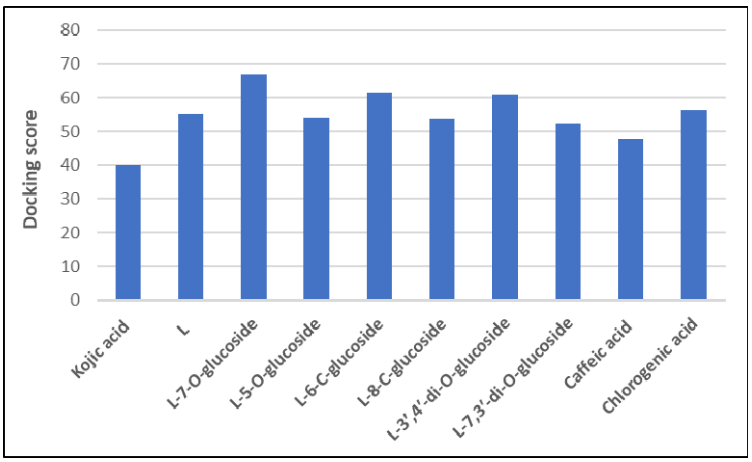

Figure 2. Docking scores for Luteolin (**L**) derivatives, caffeic and chlorogenic acids, against human tyrosinase related protein 1 (PDB ID 5M8M).

Table 1. Intermolecular interactions between ligands and 5M8M and docking results.

Ligand	Score	RMSD	Interacting Group (Chain A)	Hydrogen Bond	Length (Å)
KOJ A514 (grey)	−39.79	0.06	HIS215, HIS192, THR391, PRO395, SER394, PHE400, GLN390, GLY388, GLY389, LEU382, HIS381, ARG374, LEE379, ASN378, HIS377, TYR362	Osp^3 (O2)-Osp^3 SER394	2.889
				Osp^2 (O3)-Nsp^2 HIS215	3.203
L (magenta rose)	−55.02	0.02	ARG374, TYR362, HIS377, HIS401, PHE220, HIS224, ARG321, LEU382, ASN378, HIS381, PHE400, HIS215, HIS192, PRO395, SER394, GLY388, GLY389, THR391, GLN390, HIS392	Osp^2 (O3)-Nsp^2 ARG374	2.969
				Osp^3 (O2)-Nsp^2 ARG374	2.846
				Osp ^{3}(O2)-Nsp^2 ARG374	2.885
				Osp^3 (O2)-Nsp^2 ARG321	3.174
				Osp^2 (O1)-Osp^3 THR391	3.166
				Osp^3 (O5)-Nsp^2 HIS377	2.982
				Osp^3 (O5)-Nsp^2 HIS215	3.161
				Osp^3 (O6)-Nsp^2 HIS192	3.134
				Osp^3 (O6)-Osp^3 SER394	2.968
				Osp^3 (O6)-Nsp^2 HIS381	3.387
L-7-*O*-glucoside (green)	−66.76	1.27	HIS192, HIS224, PHE220, HIS215, HIS404, THR391, PHE400, SER394, GLU360, GLN390, GLY388, THR387, HIS377, ASN378, HIS381, GLY389, TYR362, ARG374, GLY386, LEU384, ASN385, LEU382, PHE383, ASN318, ARG321	Osp^2 (O9)-Nsp^2 ARG374	2.825
				Osp^3 (O8)-Nsp^2 ARG374	2.552
				Osp^3 (O6)-Nsp^2 ASN318	2.967
				Osp^3 (O6)-Nsp^2 ASN385	3.103
				Osp^3 (O4)-Nsp^2 GLY386	3.039
				Osp^3 (O4)-Osp^2 GLY386	3.050
				Osp^3 (O10)-Nsp^2 HIS381	3.173
				Osp^3 (O10)-Osp^3 SER394	2.906
				Osp^3 (O11)-Nsp^2 HIS215	3.985
				Osp^3 (O11)-Nsp^2 HIS381	3.084
L-5-*O*-glucoside (light blue)	−54.21	0.13	ARG321, ARG374, LEU382, TYR362, ASN378, HIS381, HIS377, GLU360, HIS404, PHE220, HIS224, HIS192, HIS215, PHE400, THR391, SER394, GLN390, GLY388, GLY389	Osp^2 (O9)-Nsp^2ARG374	3.038
				Osp^2 (O9)-Nsp^2ARG374	3.030
				Osp^3(O5)-Nsp^2ARG374	2.820
				Osp^3(O5)-Nsp^2ARG321	2.713
				Osp^2(O7)-Osp^3THR391	2.744
				Osp^3(O11)-Nsp^2HIS215	3.103
				Osp^3(O11)-Nsp^2HIS381	3.225
				Osp^3(O10)-Osp^3SER394	2.642
L-6-C-glucoside (purple)	−61.55	0.15	ARG374, TYR362, GLU360, HIS377, ASN378, HIS404, PHE220, HIS224, HIS215, HIS192, HIS392, THR391, SER394, GLN390, GLY388, GLY389, HIS381, LEU382, ARG321, ASN318	Osp^3(O9)-Nsp^2 ARG374	2.423
				Osp^3(O9)-Nsp^2 ARG374	3.156
				Osp^3(O6)-Nsp^2 ARG374	3.110
				Osp^3(O6)-Nsp^2 ARG321	3.115
				Osp^3(O2)-Nsp^2 ARG321	2.990
				Osp^3(O2)-Nsp^2 ARG321	2.901
				Osp^3(O1)-Nsp^2 ARG321	2.967
				Osp^3(O4)-Nsp^2 ARG321	2.831
				Osp^3(O10)-Osp^3 SER394	2.502
				Osp^3(O11)-Nsp^2 HIS381	3.248
				Osp^3(O11)-Nsp^2HIS215	3.113
				Osp^2(O8)-Osp^3THR391	3.180
L-8-C-glucoside (brown)	−53.81	0.03	HIS192, HIS392, SER394, PHE400, THR391, GLN390, GLY388, GLY389, HIS381, LEU382, ARG321, ARG374, TYR362, ASN378, HIS377, GLU360, PHE220, HIS215, HIS204, HIS224	Osp^2 (O9)- Nsp^2ARG374	2.884
				Osp^2 (O8)-Nsp^2ARG374	2.569
				Osp^2 (O8)-Nsp^2ARG374	2.592
				Osp^2 (O8)-Nsp^2 ARG321	3.083
				Osp^3 (O10)-Nsp^2 HIS215	2.751

				Osp^3 (O11)-Nsp^2 HIS192	3.134
				Osp^3 (O11)-Osp^3 SER394	3.060
				Osp^3 (O2)-Osp^3 THR391	2.451
L-3′,4′-di-*O*-glucoside (red brown)	−60.91	2.68	GLU216, HIS215, ASP212, VAL211, VAL196, GLY209, LYS198, LYS197, LEU293, HIS392, THR391, GLN390, GLY388, GLY389, ARG321, LEU382, HIS381, LEU379, ASN378, ARG374, HIS377, TYR362	Osp^2 (O3)-Nsp^2 HIS392	2.789
				Osp^3 (O4)-Osp^3 ASP212	3.001
				Osp^2 (O1)-Osp^3 THR391	2.707
				Osp^3 (O12)-Osp^3 THR391	3.271
				Osp^3 (O13)-Osp^3 THR391	2.906
				Osp^3 (O13)-Nsp^2 THR391	3.050
				Osp^3 (O13)-Osp^2 GLY389	2.856
				Osp^3 (O14)-Osp^2 ASN378	3.046
				Osp^3 (O15)-Osp^3 TYR362	2.656
				Osp^3 (O16)-Nsp^2 ARG374	3.307
				Osp^3 (O16)-Nsp^2 ARG374	2.671
				Osp^3 (O9)-Nsp^2 ARG321	3.022
				Osp^3 (O9)-Nsp^2 ARG321	2.909
				Osp^3 (O10)-Nsp^2 ARG374	3.073
L-7,3′-di-*O*-glucoside (blue)	−52.44	2.43	LEU293, HIS392, THR391, GLN390, GLY389, HIS381, LEU382, ARG321, ASN378, HIS377, ARG374, GLU360, TYR362, TYR348, GLU216, HIS215, GLU210, VAL211, ASP212, GLY209, VAL196, LYS198, LYS197	Osp^2 (O13)-Osp^3 THR391	2.836
				Osp^2 (O13)-Nsp^2 THR391	3.192
				Osp^3 (O14)-Osp^2 VAL196	2.698
				Osp^3 (O10)-Osp^2 VAL196	3.094
				Osp^3 (O10)-Osp^2 VAL211	2.913
				Osp^3 (O10)-Osp^2 GLY209	3.240
				Osp^3 (O8)-Osp^2 VAL211	2.867
				Osp^3 (O8)-Osp^2 GLY209	2.823
				Osp^3 (O7)-Osp^3 GLU216	2.674
				Osp^3 (O12)-Osp^3 GLU216	3.054
				Osp^3 (O1)-Osp^3 THR391	3.157
				Osp^3 (O5)-Osp^3 TYR362	2.920
				Osp^3 (O5)-Osp^2 ASN378	3.089
				Osp^3 (O4)-Nsp^2 ARG374	3.148
				Osp^3 (O4)-Nsp^2 ARG374	2.554
Caffeic acid (orange brown)	−47.63	0.05	PHE220, HIS215, HIS224, HIS192, THR391, PRO395, HIS404, SER394, PHE400, GLN390, GLY388, GLY389, LEU382, HIS381, ASN378, HIS307, ARG374, TYR362, GLU360	Osp^3 (O3)-Nsp^2 ARG374	3.146
				Osp^2 (O4)-Nsp^2 ARG374	2.860
				Osp^2 (O4)-Nsp^2 ASN378	3.034
				Osp^3 (O1)-Nsp^2 HIS377	3.195
				Osp^3 (O1)-Nsp^2 HIS215	3.019
				Osp^3 (O1)-Nsp^2 HIS381	3.374
				Osp^3 (O2)-Osp^3 SER394	2.424
Chlorogenic acid (light purple)	−56.08	2.05	ARG321, ARG374, TYR362, LEU382, ASN378, HIS377, GLU360, HIS381, HIS404, PHE220, HIS224, HIS215, PHE400, GLY389, GLY388, GLN390, SER394, THR391, PRO395, HIS192	Osp^3 (O9)-Nsp^2 HIS381	3.289
				Osp^3 (O9)-Nsp^2 HIS215	3.031
				Osp^3 (O8)-Osp^3 SER394	2.523
				Osp^2 (O7)-Nsp^2 ARG374	2.854
				Osp^2 (O7)-Nsp^2 ARG374	3.072
				Osp^3 (O2)-Nsp^2 ARG321	3.107
				Osp^3 (O2)-Nsp^2 ARG321	2.738
				Osp^3 (O4)-Nsp^2 ARG321	2.862
				Osp^3 (O3)-Osp^2 GLY389	2.817

Figure 3 illustrates the arbitrary numbering scheme for constitutive atoms of investigated structures, as given for the most stable conformers of each structures, obtained after energy minimization using Spartan Software [8]. Figure 4 depicts the intermolecular interactions of investigated ligands with 5M8M, illustrating the hydrogen bonds formed by the hydroxyl (O sp^3) or carboxyl group (O sp^2) of investigated structures and amino acids residues from the binding pocket of the protein fragment, directly interacting.

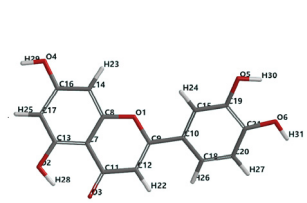

(**a**) Luteolin (**L**)

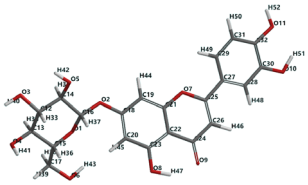

(**b**) **L**-7-*O*-glucoside

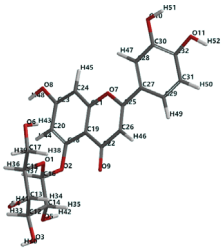

(**c**) **L**-5-*O*-glucoside

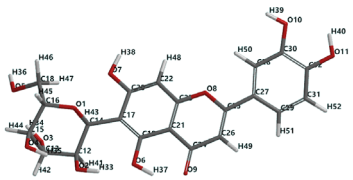

(**d**) **L**-6-C-glucoside

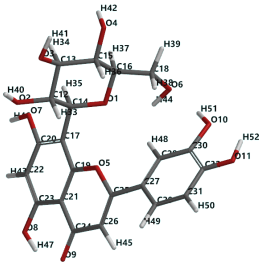

(**e**) **L**-8-C-glucoside

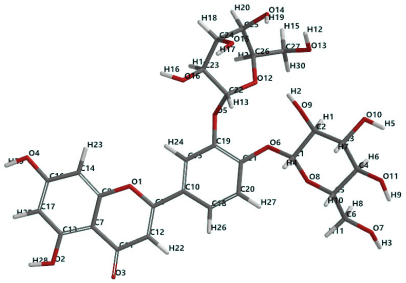

(**f**) **L**-3′,4′-di-*O*-glucoside

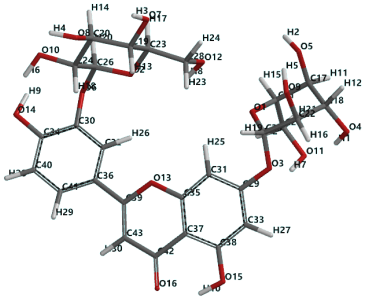

(**g**) **L**-7,3′-di-*O*-glucoside

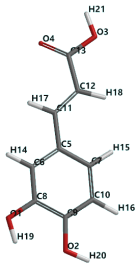

(**h**) Caffeic acid

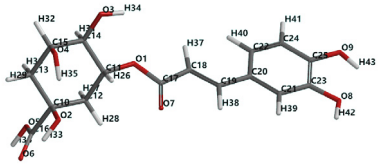

(**i**) Chlorogenic acid

Figure 3. Atoms labels numbering for: (**a**) **L**; (**b**) **L**-7-O-glucoside; (**c**) **L**-5-O-glucoside; (**d**) **L**-6-C-glucoside; (**e**) **L**-8-C-glucoside; (**f**) **L**-3′,4′-di-*O*-glucoside; (**g**) **L**-7,3′-di-*O*-glucoside; (**h**) caffeic acid; (**i**) chlorogenic acid.

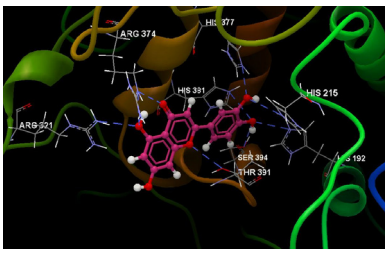

(**a**) Hydrogen bond interactions of **L** with 5M8M

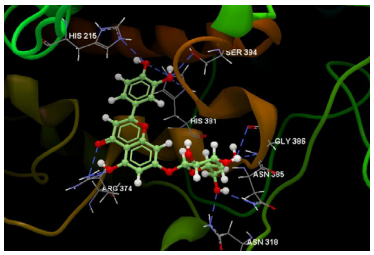

(**b**) Hydrogen bond interactions of **L**-7-*O*-glucoside with 5M8M

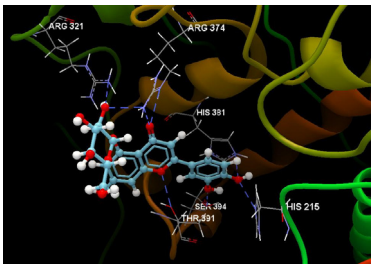

(**c**) Hydrogen bond interactions of **L**-5-*O*-glucoside with 5M8M

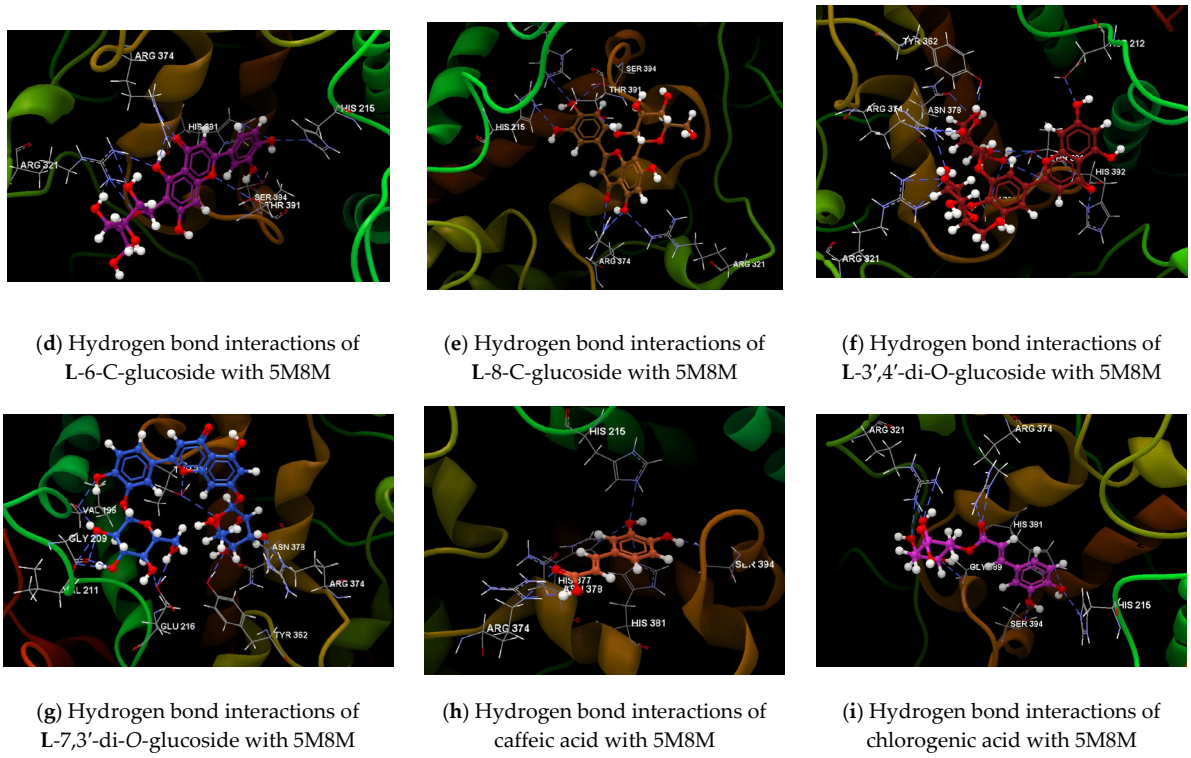

(**d**) Hydrogen bond interactions of **L**-6-C-glucoside with 5M8M

(**e**) Hydrogen bond interactions of **L**-8-C-glucoside with 5M8M

(**f**) Hydrogen bond interactions of **L**-3′,4′-di-O-glucoside with 5M8M

(**g**) Hydrogen bond interactions of **L**-7,3′-di-*O*-glucoside with 5M8M

(**h**) Hydrogen bond interactions of caffeic acid with 5M8M

(**i**) Hydrogen bond interactions of chlorogenic acid with 5M8M

Figure 4. Intermolecular interactions of investigated ligands with 5M8M, as hydrogen bonds formed by: (**a**) Luteolin (**L**); (**b**) **L**-7-*O*-glucoside; (**c**) **L**-5-*O*-glucoside; (**d**) **L**-6-C-glucoside; (**e**) **L**-8-C-glucoside; (**f**) **L**-3′,4′-di-*O*-glucoside; (**g**) **L**-7,3′-di-*O*-glucoside; (**h**) caffeic acid and (**i**) chlorogenic acid.

4. Discussion

Very extensive studies summing 582 extracted samples obtained from 370 plants [9] indicated several plants derived products and specific phytocompounds (there were investigated 118 separate compounds) as being able to act as inhibitors of B16F-10 melanoma metastatic cell line viability. Therefore, the most effective plant derived products were *Mangifera indica*-barks, leaves and seeds extracts, *Annona cherimola*, *Annona muricata* and *Annona squamosa*-bark, leaves, stems and twigs extracts, *Anthriscus sylvestris*-fruits, leaves and roots extracts, *Osmorhiza aristata*-aerial parts extracts, *Araucaria heterophylla*-leaves extracts, *Tylophora ovata* and *Tylophora tanakae*-fresh leaves, twigs and aerial parts extracts, *Crepidiastrum lanceolatum*-aerial parts extracts, *Garcinia subelliptica*-barks extracts, *Luffa acutangula* and *Momordica cochinchinensis*-seeds extracts, *Juniperus rigida* and *Thuja occidentalis*-leaves extracts, *Persea americana*-leaves extracts and *Coptis japonica*-rhizomes extracts. Plant derived products inhibitory activity (EC_{50}) was mostly evaluated as less than 100 μg/mL (70%), 12% of them being evaluated as less than 12.5 μg/mL. Moreover, lignan compounds were proved as the most effective inhibitors of B16F-10 melanoma metastatic cell line viability; deoxypodophyllotoxin and morensin proved the most augmented antiproliferative effects being evaluated at EC_{50} = 0.21 and 0.23 μg/mL respectively. Other polyphenols compounds such as apigenin (EC_{50} = 25 μg/mL), luteolin (EC_{50} = 21 μg/mL), baicalein (EC_{50} = 11 μg/mL), gallic acid and derivates (EC_{50} = 2–9 μg/mL) and hydroxycinnamic acid derivates, also were proved to provide certain anti-proliferative effects against B16F-10 melanoma metastatic cell line viability [9].

The present work suggests certain cytotoxic and antiproliferative activity of 40% ethanolic extract (Slae26) from *Stokesia laevis* plant species (the aerial part), upon normal murine fibroblast cell line L929 and murine melanoma cell line B16; also, HPTLC analysis of Slae26 indicated the presence of two major polyphenols subclasses, caffeic acid and luteolin derivates, punctually the predominance of caffeic acid, chlorogenic acid, luteolin

and luteolin-7-*O*-glucoside [5]. Also, the docking results indicated similar interactions for the co-crystallized kojic acid and the nine vegetal compounds tested (punctually, Luteolin (**L**), **L**-7-*O*-glucoside, **L**-5-*O*-glucoside, **L**-6-C-glucoside, **L**-8-C-glucoside, **L**-3′,4′-di-*O*-glucoside, **L**-7, 3′-di-*O*-glucoside, Caffeic acid and Chlorogenic acid); furthermore, there were noticed interactions with the same amino acid residues, by hydrogen bonds formed with O sp^3 of SER394, and N sp^2 of HIS215, respectively, except for di-glucosides. In addition, due to the numerous hydroxyl groups of our investigated structures, more interactions in the protein-complex occur and higher docking score are revealed. Therefore, docking results suggest the ability of luteolin and caffeic acid derivatives to act as potential skin melanoma cancer inhibitors.

5. Conclusions

For the first time in literature data, potential cytotoxic and anti-proliferative effects of the ethanolic extract from *S. aster* on both, normal murine fibroblast cell line L929, and murine melanoma cell line B16 have been proved. Molecular docking approach on the major components of Slae26 against human tyrosinase receptor has reveal possible melanogenesis inhibition.

Author Contributions: Conceptualization, L.C.P. and A.S.; methodology, A.S. and G.N.; software, L.P., A.S. and B.A.; validation, G.N. and L.P.; formal analysis, B.A.; investigation, A.S., G.N. and I.T.; resources, G.N.; data curation, L.C. P.; writing—original draft preparation, A.S.; writing—review and editing, L.C.P.; visualization, G.N.; supervision, L.C.P.; project administration, L.C.P.; funding acquisition, L.C.P. All authors have read and agreed to the published version of the manuscript.

Funding: This work was supported by the ANCSI POC-A1-A1.2.3-G-2015 (Project ID P_40_406, SMIS 105542, Contract no. 60/05.09.2016).

Institutional Review Board Statement: Not applicable.

Informed Consent Statement: Not applicable.

Conflicts of Interest: The authors declare no conflict of interest.

References

1. Domingues, B.; Lopes, J.M.; Soares, P.; Populo, H. Melanoma treatment in review. *Immunotargets Ther*. **2018**, *7*, 35–49.
2. Skin Cancer Statistics. Available online: https://www.wcrf.org/dietandcancer/cancer-trends/skin-cancer-statistics (accessed on 24 October 2020).
3. Kalal, B.S.; Upadhya, D.; Pai, V.R. Chemotherapy resistance mechanisms in advanced skin cancer. *Oncol. Rev.* **2017**, *11*, 326, doi:10.4081/oncol.2017.326.
4. Chinembiri, N.T.; du Plessis, L.H.; Gerber, M.; Hamman, J.H.; du Plessis, J. Review of natural compounds for potential skin cancer treatment. *Molecules* **2014**, *19*, 11679–11721.
5. Pirvu, L.; Neagu, G.; Terchescu, I.; Albu, B.; Stefaniu, A. Comparative studies of two vegetal extracts from *Stokesia laevis* and *Geranium pratense*: Polyphenol profile, cytotoxic effect and antiproliferative activity. *Open Chem.* **2020**, *18*, 488–502.
6. Lai, X.; Wichers, H.J.; Soler-Lopez, M.; Dijkstra, B.W. Structure of human tyrosinase related protein 1 reveals a binuclear zinc active site important for melanogenesis. *Angew. Chem. Int. Ed.* **2017**, *56*, 9812–9815, doi:10.1002/anie.201704616.
7. Lai, X.; Soler-Lopez, M.; Wichers, H.J.; Dijkstra, B.W. Crystal Structure of Human Tyrosinase Related Protein 1 in Complex with Kojic Acid; PDB ID: 5M8M. Deposited on: 2016-10-29. Available online: https://www.rcsb.org/structure/5M8M (accessed on 5 November 2020).
8. Shao, Y.; Molnar, L.F.; Jung, Y.; Kussmann, J.; Ochsenfeld, C.; Gilbert, A.T.B.; Slipchenko, L.V.; Levchenko, S.V.; O'Neill, D.P.; DiStasio, R.A., Jr.; et al. Advances in methods and algorithms in a modern quantum chemistry program package. *Phys. Chem. Chem. Phys.* **2006**, *8*, 3172–3191.
9. Kinjo, J.; Nakano, D.; Fujioka, T.; Okabe, H. Screening of promising chemotherapeutic candidates from plants extracts. *J. Nat. Med.* **2016**, *70*, 335–360.